L-band InSAR Snow Water Equivalent Retrieval Uncertainty Increases with Forest Cover Fraction*

R. Bonnell[1+], K. Elder[2#], D. McGrath[1#], H.P. Marshall[3], B. Starr[2], N. Adebisi[3], R. Palomaki[4], Z. Hoppinen[3,5]
Colorado State University[1], U.S. Forest Service Rocky Mountain Research Station[2], Boise State University[3], University of Colorado[4], & Cold Regions Research & Engineering Laboratory[5]
*In Review at Geophysical Research Letters, [+]Presenting Author: rbonnell@colostate.edu, [#]Contributed Equally

I. Summary

- We evaluated changes in SWE (ΔSWE) retrievals calculated from eight repeat InSAR pairs collected by NASA UAVSAR during the NASA SnowEx 2021 Campaign at the Fraser Experimental Forest (FEF), CO.
- ΔSWE retrievals were unbiased and accurate (RMSE = 14–17 mm) in forest cover fractions (FCF) <0.40, but accuracy decreased (RMSE = 33–40 mm) and bias was introduced at FCF >0.50.
- L-band InSAR appears to be a viable path towards snowpack monitoring below sparse to moderate forest cover.

II. SnowEx21 at FEF

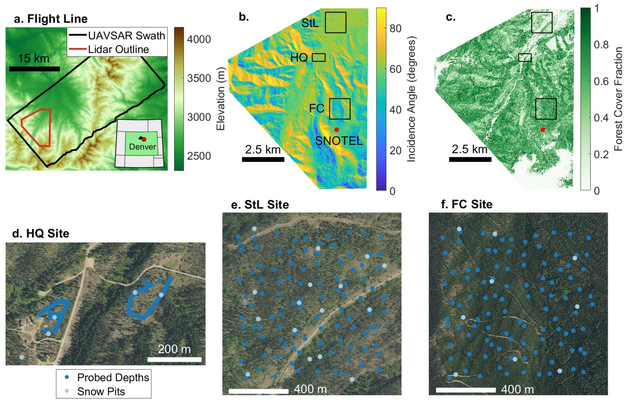

Figure 1: (a) DEM of the Fraser, CO UAVSAR swath with inset map of Colorado. (b) UAVSAR local incidence angles from the 052° heading and (c) lidar-derived FCF over FEF. NAIP imagery showing in situ measurement locations at the (d) HQ, (e) StL, and (f) FC field sites.

a. Study Questions

1. What is the accuracy of repeat L-band InSAR ΔSWE retrievals in both forested and open environments?
2. Can cumulative InSAR ΔSWE retrievals accurately capture the spatial distributions of snow documented by lidar snow depths?

b. Datasets

UAVSAR
- Unwrapped phase and coherence from headings 052° (Figure 1a) and 233° (NASA UAVSAR, 2021)

In Situ
- Snow pits (Mason et al., 2024) and probed depths at Headquarters (HQ), St. Louis Creek (StL), and Fool Creek (FC) field sites (Figure 1d–f)
- Fool Creek SNOTEL (ID 1186; Figure 1b)

Airborne Lidar
- DEM (Adebisi et al., 2022a) used to calculate local incidence angles (Figure 1b)
- Lidar snow depths (Adebisi et al., 2022b) converted to normalized snow depths
- Vegetation heights (Adebisi et al., 2022c) converted to FCF (Figure 1c)

III. Methods

1. Identify and remove atmospheric phase ramps (Figure 2).
2. Calculate local incidence angles from lidar DEM (Figure 1b).
3. Estimate snow surface density and relative permittivity (Kovacs et al., 1995) from snow pits. Assumed dry snow conditions based on snow pit temperatures (Figure 3).
4. Calculate ΔSWE from unwrapped phase, relative permittivity/density, and local incidence angle (Guneriussen et al., 2001).
5. Evaluate ΔSWE with in situ observations.
6. Normalize and integrate ΔSWE across the eight-week time series and compare with normalized lidar snow depths.

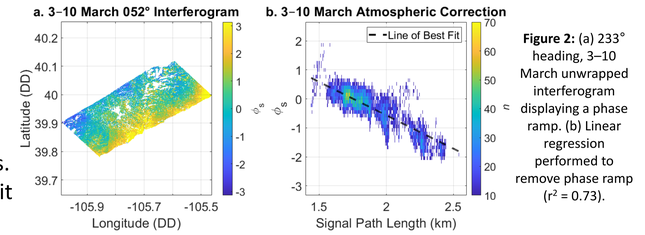

Figure 2: (a) 233° heading, 3–10 March unwrapped interferogram displaying a phase ramp. (b) Linear regression performed to remove phase ramp (r^2 = 0.73).

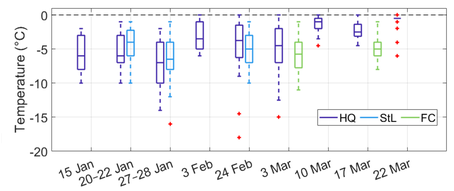

Figure 3: Box plots of snow pit temperatures collected at the three field sites. We note that surface temperatures tend to be cooler, whereas temperatures near the snow-ground interface tend to be warmer.

IV. Results

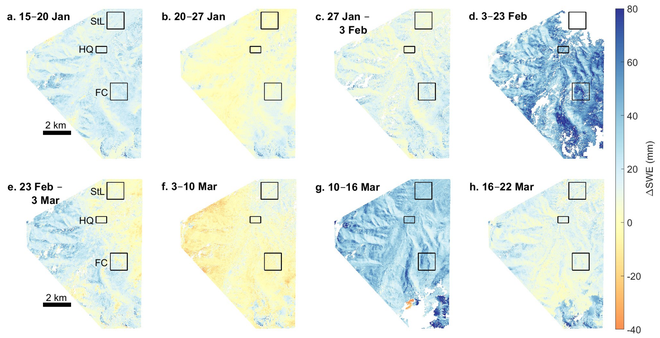

Figure 4: UAVSAR ΔSWE retrievals for each 052° heading InSAR pair. Field sites are outlined in black.

UAVSAR ΔSWE Retrievals
- ΔSWE retrievals reveal complex spatial patterns over the forested terrain (Figure 4).
- Mean site-wide ΔSWE retrievals were similar between polarizations and headings for each interval (Table 1).

Table 1: Site-wide mean UAVSAR ΔSWE ± one standard deviation (mm) for each of the four polarizations and flight headings. A hyphen indicates no data.

Date Interval	052° HH	233° HH	052° HV	233° HV	052° VH	233° VH	052° VV	233° VV
15–20 Jan	17 ± 8	-	17 ± 8	-	18 ± 9	-	17 ± 8	-
20–27 Jan	5 ± 7	-	-	-	7 ± 8	-	5 ± 7	-
27 Jan – 3 Feb	15 ± 10	16 ± 9	16 ± 10	17 ± 9	16 ± 10	16 ± 9	13 ± 9	15 ± 8
3–23 Feb	-	-	-	-	46 ± 17	-	-	-
23 Feb – 3 Mar	10 ± 12	-	12 ± 13	-	11 ± 13	-	13 ± 12	-
3–10 Mar	–4 ± 11	1 ± 11	–6 ± 11	4 ± 11	–3 ± 11	4 ± 11	0 ± 10	3 ± 10
10–16 Mar	36 ± 13	32 ± 11	33 ± 13	31 ± 11	34 ± 15	31 ± 11	34 ± 14	31 ± 11
16–22 Mar	12 ± 11	11 ± 8	18 ± 12	20 ± 10	17 ± 11	22 ± 10	14 ± 11	17 ± 9

Evaluating ΔSWE Retrievals
- Single pair ΔSWE retrievals were unbiased for FCF <0.40 and cumulative SWE was within 50 mm accuracy for all three field sites (Figure 5a).
- RMSE increased from ~15 mm at FCF <0.40 to 26 mm for 0.40–0.50 FCF, and approached 40 mm for FCF >0.50 (Figure 5f).
- Normalized depth/SWE yielded similar distribution patterns across different elevation ranges (Figure 6e).

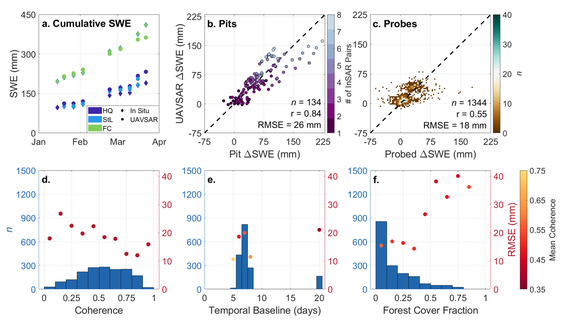

Figure 5: (a) Median SWE measured/estimated from in situ measurements compared with median integrated 052° heading UAVSAR SWE for each field site. (b) UAVSAR ΔSWE evaluated in situ snow pit ΔSWE measurements. (c) UAVSAR ΔSWE evaluated against ΔSWE estimated from probed depth measurements. Histograms and RMSE for each histogram bin for (d) coherence, (e) temporal baseline, and (f) FCF.

- Normalized SWE was positively biased relative to normalized depth for FCF >0.60 (Figure 6d).
- Normalized SWE exhibied clear artifacts related to the SAR viewing geometry (Figure 6f).

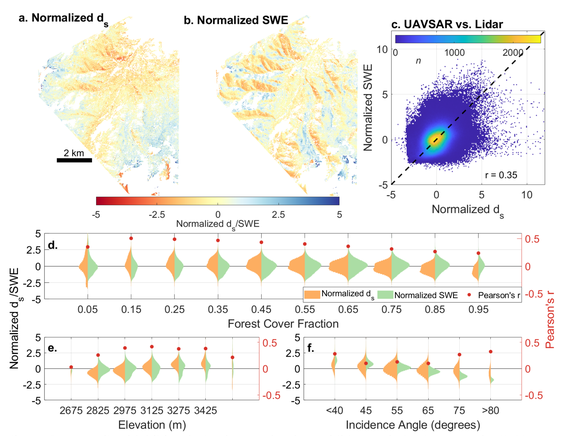

Figure 6: Normalized (a) lidar-derived snow depths and (b) cumulative integrated UAVSAR SWE. (c) 2-d histogram showing the comparison between normalized lidar depths and normalized UAVSAR SWE. Violin plots showing the histogram distributions of normalized lidar snow depth and normalized UAVSAR SWE and r binned by (d) forest cover fraction, (e) elevation, and (f) local incidence angle.

V. Implications for NISAR

Forest Backscattering Characteristics
- Based on polarimetric decomposition, there were no detectable differences between the distributions of radar backscatter properties for any FCF interval >0.10 (Figure 7). Even meadows exhibited volume scattering.

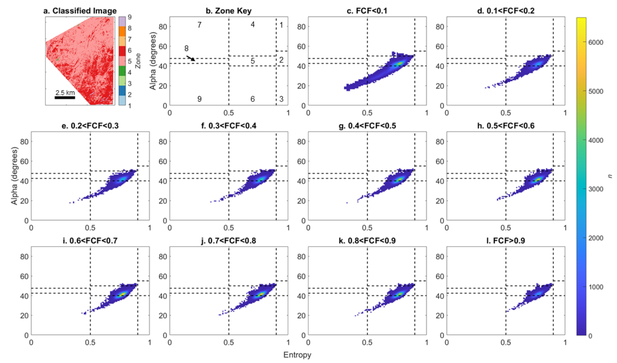

Figure 7: Polarimetric decomposition analysis following Cloude & Pottier (1997). (a) Site-wide classification for FEF. (b) Classification zones. (c–l) 2-d histogram plots of Alpha-Entropy distributions binned by FCF.

Snow in the trees
- The positive bias of normalized UAVSAR SWE, compared to normalized lidar depths, may be partly explained by canopy-intercepted snow. Lidar snow depths do not include canopy snow. Snow was observed in the canopy for March 2021 surveys and was documented throughout FEF via PlanetScope imagery (Figure 8).

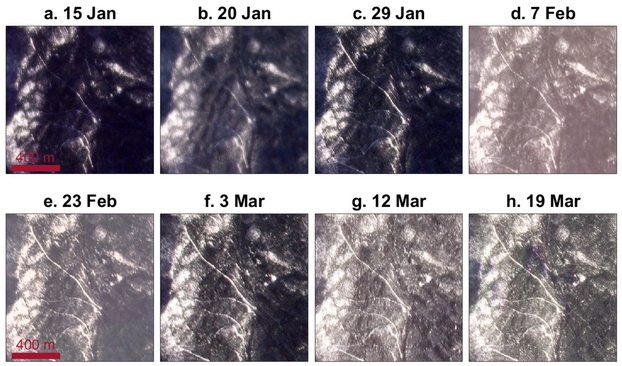

Figure 8: PlanetScope satellite imagery of the FC field site acquired on or near UAVSAR acquisition dates. Surveyors observed snow in the trees on 10 February, and 10, 17, and 22 March 2021.

VI. Acknowledgements & References

Thank you to the SnowEx leadership team! R.B. acknowledges NASA FINESST award 80NSSC20K1624. K.E. and B.S. acknowledge NASA award NNG210B37A. D.M. and H.P.M. acknowledge NASA awards 80NSSC18K1405 and 80NSSC22K1113.
We are grateful to the developers of *uavsar_pytools*, including J. Tarricone.

1. Adebisi et al. (2022a). SnowEx20-21 QSI Lidar DEM 0.5m UTM Grid, Version 1 [data set]. NASA NSIDC DAAC.
2. Adebisi et al. (2022b). SnowEx20-21 QSI Lidar Snow Depth 0.5m UTM Grid, Version 1 [data set]. NASA NSIDC DAAC.
3. Adebisi et al. (2022c). SnowEx20-21 QSI Lidar Vegetation Height 0.5m UTM Grid, Version 1 [data set]. NASA NSIDC DAAC.
4. Cloude & Pottier (1997) An entropy based classification scheme for land applications of polarimetric SAR. *IEEE Trans Geosci Remote Sens*, 35(1), 68-78.
5. Guneriussen et al. (2001). InSAR for estimation of changes in snow water equivalent of dry snow. *IEEE Trans Geosci Remote Sens*, 39(10), 2101-2108.
6. Kovacs et al. (1995). The in-situ dielectric constant of polar firn revisited. *Cold Reg Sci Technol*, 23(3), 245-256.
7. Mason et al. (2024). SnowEx21 Time Series Snow Pits, Version 1 [data set]. NASA NSIDC.
8. NASA UAVSAR (2021). Fraser, Colorado Flight Line [data set]. NASA ASF DAAC.